IEEE Access
Multidisciplinary ⋮ Rapid Review ⋮ Open Access Journal

Received 10 April 2024, accepted 26 April 2024, date of publication 2 May 2024, date of current version 14 May 2024.

*Digital Object Identifier 10.1109/ACCESS.2024.3396128*

RESEARCH ARTICLE

# Electromagnetic Fields Induced by Three-Dimensional Short Ocean Waves in a Horizontally Layered Seabed

**RONGHUA TAO[1], BAOQIANG ZHANG[2], CHUN ZHOU[2], AND HE QIAO[2]**
[1]Institute of Remote Sensing, Navy Submarine Academy, Qingdao 266000, China
[2]Qingdao Institute of Collaborative Innovation, Qingdao 266075, China
Corresponding author: Baoqiang Zhang (baoqiangouc@163.com)

**ABSTRACT** An accurate model is needed to simulate the electromagnetic fields induced by short-period ocean waves to study the influence of the induced fields on the data set of marine magnetotelluric (mMT), marine controlled source electromagnetic (mCSEM), and marine airborne (low altitude) magnetic anomaly detection (MAD). By using a three-dimensional (3-D) linear wave model and directly solving linear equations derived from Maxwell's equations and boundary conditions of a horizontal layered seabed, we obtained analytical solutions of the six components of the electromagnetic fields induced by three components of the velocity of ocean waves and three components of geomagnetic fields. In addition to horizontal currents induced by the horizontal velocity and vertical geomagnetic field, the contributions from the horizontal current induced by the vertical velocity and horizontal geomagnetic field and vertical current were considered in the governing equations. On the basis of the solutions, we studied how the geomagnetic field and wind fields affect the relationship between the two horizontal components and between the horizontal and vertical components of the electromagnetic fields at the sea surface. We simulated the influence of water depth and wind fields on the distribution of the spectrum and time series of the induced fields by using a typical wave spectrum and directional spectrum. Finally, the possibility of detecting seafloor conductivity structures by using the electromagnetic response of short ocean waves was also discussed.

**INDEX TERMS** Electromagnetic fields, frequency spectrum, motional induction, ocean waves, time series.

## I. INTRODUCTION

The electromagnetic field can be generated by the electric currents induced by ocean movement across the Earth's magnetic field. This phenomenon, called motional induction, has interested physicists since the speculations of Faraday (1832). Motional induction due to surface gravity waves, such as ocean waves and swells, which have short periods compared to other oceanic flows, has attracted increasing attention in some ocean applications. These induced fields contaminate marine magnetotelluric (mMT), marine controlled source electromagnetic (mCSEM) and magnetic surveying signals used for geology and hydrocarbon exploration studies [1], [2], [3], [4], [5], [6], [7], [8]. Similarly, the induced magnetic fields dominate the noise level of magnetometers, thus affecting the performance of marine magnetic anomaly detection (MAD) at low altitude [9], [10], [11], [12], [13].

To study this problem, an accurate model that simulates the electromagnetic fields of short-period ocean waves is needed [14]. Reference [15] was the first to obtain an exact solution by directly solving Maxwell's equations using the boundary conditions of a conducting half-space. Subsequently, scientists turned their interest in motional induction into long waves, such as tsunamis, ocean tides, large-scale low-frequency oceanic flows, baroclinic waves, and ocean circulation. Many studies are given in review papers [16].

The associate editor coordinating the review of this manuscript and approving it for publication was Wuliang Yin.

In this paper, we focus on the modeling of electromagnetic fields related to short ocean waves. During modeling in past studies, two-dimensional ocean waves were assumed to be a single wave of a single discrete frequency traveling in a single direction. However, when deriving the solutions of the induced fields, mostly the horizontal current induced by a horizontal velocity and the vertical geomagnetic field was considered. Contributions from horizontal currents that occurred due to vertical velocities and horizontal geomagnetic fields and vertical currents were ignored. The main work of this paper is as follows. (1) By directly solving linear equations derived from Maxwell's equations, we obtain the analytical solutions of the six components of electromagnetic fields, which are induced by three components of velocity and three components of geomagnetic fields. (2) The effects of the geomagnetic field and wind fields on the relationship between the various components of the induced fields at the sea surface is studied. (3) The spectrum and time series of the motional fields are simulated, and the influence of the wind field and underwater depth on its distribution is studied. (4) Finally, the possibility of detecting seafloor conductivity structures by using the electromagnetic response of short ocean waves is discussed.

## II. THEORY OF MOTION INDUCTION

### A. MODEL AND FIELD EQUATION

We build a mathematical model of 3-D ocean waves with a horizontally layered electrical conductivity structure, as shown in Fig. 1. Layers 0 and 1 correspond to the air and sea, respectively. The thicknesses of seawater and layers beneath the seafloor are $h_1, h_2, h_j, \cdots, h_{N-1}$, respectively. The electrical conductivities are $\sigma_0, \sigma_1, \sigma_2, \sigma_j, \cdots, \sigma_N$, respectively. Air and Layer $N$ extend indefinitely. We employ a local Cartesian coordinate system $(x, y, z)$, the $z$-axis is taken to be vertically downward direction and the $x$- and $y$-axes form a horizontal plane. $z = 0$ and $z = h_1$ correspond to the sea surface and seafloor, respectively. The source of electromagnetic fields is assumed to be motional induction from the 3-D ocean waves in the geomagnetic field. $a$ is the amplitude of ocean waves at the sea surface. $\alpha$ denotes wind direction. Moreover, the geomagnetic field vector can be written as:

$$\begin{aligned}\boldsymbol{F} &= F_x\vec{i} + F_y\vec{j} + F_z\vec{k} \\ &= F\left(\cos I\cos\phi\,\vec{i} + \cos I\sin\phi\,\vec{j} + \sin I\,\vec{k}\right)\end{aligned} \tag{1}$$

where $\vec{i}$, $\vec{j}$, $\vec{k}$ are unit vectors in the $x$, $y$ and $z$ directions. $I$ is the geomagnetic inclination. $\phi$ denotes the deviation between the geomagnetic north and $x$-axis. $F$ is the intensity of the geomagnetic field. For the time and spatial scale, we assume that $F$ is constant in time and space.

The motional electric field $\boldsymbol{E}$ and magnetic flux density $\boldsymbol{B}$ satisfy Maxwell equations:

$$\nabla \times \boldsymbol{E} = -\frac{\partial \boldsymbol{B}}{\partial t} \tag{2}$$

$$\frac{1}{\mu_0}\nabla\times\boldsymbol{B} = \boldsymbol{j}^{\mathbf{ext}} + \sigma\boldsymbol{E} + \varepsilon\frac{\partial \boldsymbol{E}}{\partial t} \tag{3}$$

where $\mu_0 (= 4\pi \times 10^{-7}\mathrm{H/m})$ is the magnetic permeability, $\varepsilon (\approx 8.85 \times 10^{-12}\mathrm{F/m})$ is the permittivity of the vacuum, and $\sigma$ is the electrical conductivity of the medium. $\boldsymbol{j}^{\mathbf{ext}}$ is the motion-induced extrinsic source due to ocean waves. $\sigma\boldsymbol{E}$, which is the second term on the right-hand side of Equation (3), must be included in the equation because self-induction in the ocean and mutual induction with the conducting earth cannot be neglected for short-period ocean waves.

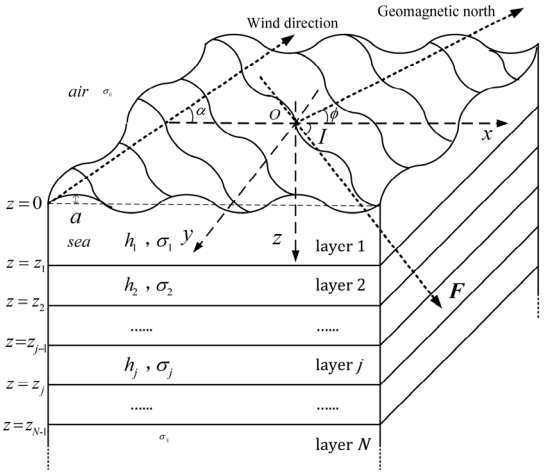


**FIGURE 1.** Three-dimensional ocean wave model with a horizontally layered electrical conductivity structure.

Regarding conductive seawater moving in the geomagnetic field and since $|\boldsymbol{B}| \ll |\boldsymbol{F}|$, the electric current $\boldsymbol{j}^{\mathbf{ext}}$ can be calculated by:

$$\boldsymbol{j}^{\mathbf{ext}} = \sigma_1 (\boldsymbol{V} \times \boldsymbol{F}) \tag{4}$$

where $\sigma_1$ is the electrical conductivity of seawater and assumed to be a constant. $\boldsymbol{V} = V_x(z)\vec{i} + V_y(z)\vec{j} + V_z(z)\vec{k}$ is the velocity vector of 3-D ocean waves. Additionally, the formulas are provided in Section II-B.

Three components of the source current $\boldsymbol{j}^{\mathbf{ext}}$ can be expressed as:

$$\begin{aligned} j_x^{\mathrm{ext}}(z) &= \sigma_1[V_y(z)F_z - V_z(z)F_y] \\ j_y^{\mathrm{ext}}(z) &= \sigma_1[V_z(z)F_x - V_x(z)F_z] \\ j_z^{\mathrm{ext}}(z) &= \sigma_1[V_x(z)F_y - V_y(z)F_x] \end{aligned} \tag{5}$$

In past studies, the horizontal current caused by the induction of horizontal velocity and the vertical geomagnetic field was mostly considered. Contributions from horizontal currents due to vertical velocities and the horizontal geomagnetic field and vertical currents have been ignored. Here, we provide a more general treatment of the source current by considering three components of the velocity of ocean waves and three components of the geomagnetic field. This indicates that the field equations and formula derivation become more complicated.

We suppose that the induced fields have a simple harmonic form of $e^{i\omega t-k_x x-k_y y}$, the intensity of which varies with propagation distance $z$. Within the realm of linear wave theory [17], the field for a single frequency is the sum of the fields due to the whole propagation directional components related to that frequency:

$$\boldsymbol{B}=\sum\left[b_x(z)\,\vec{i}+b_y(z)\,\vec{j}+b_z(z)\,\vec{k}\right]e^{i\omega t-k_x x-k_y y} \quad (6)$$

$$\boldsymbol{E}=\sum\left[e_x(z)\,\vec{i}+e_y(z)\,\vec{j}+e_z(z)\,\vec{k}\right]e^{i\omega t-k_x x-k_y y} \quad (7)$$

where $k_x = ik\cos\theta$, $k_y = ik\sin\theta$. $k$ is the wavenumber. $\omega$ is the angular frequency. $\theta$ denotes the angle between the direction of the wave component and $x$-axis.

By substituting (6) and (7) into (2) and (3), $\boldsymbol{E}$ can be eliminated, and the magnetic flux density $\boldsymbol{B}$ satisfies the following equation:

$$\frac{1}{\mu_0}\nabla^2\boldsymbol{B}-\varepsilon\frac{\partial^2\boldsymbol{B}}{\partial t}-\sigma\frac{\partial\boldsymbol{B}}{\partial t}=-\delta\nabla\times\boldsymbol{j}^{\mathbf{ext}} \quad (8)$$

Because the extrinsic source $\boldsymbol{j}^{\mathbf{ext}}$ related to ocean waves only exists in seawater, we set:

$$\delta=\begin{cases}1, & 0\le z\le h_1\\ 0, & \text{else}\end{cases} \quad (9)$$

The second-order ordinary differential equations of the three components of the magnetic flux density can be written as:

$$\begin{aligned}b_x''(z)-k_j^2 b_x(z)&=\delta p_x(z)\\ b_y''(z)-k_j^2 b_y(z)&=\delta p_y(z)\\ b_z''(z)-k_j^2 b_z(z)&=\delta p_z(z)\end{aligned} \quad (10)$$

where $k_j=\sqrt{k^2+i\omega m_j}$, $m_j=\mu_0\sigma_j+i\omega\mu_0\varepsilon_j$, $j=0,1,2,\cdots,N$, and:

$$\begin{aligned}p_x(z)&=-\mu_0\left(\nabla\times\boldsymbol{j}^{\mathbf{ext}}\right)_x\\ &=\mu_0\sigma_1\left[k_xF_xV_x(z)+k_xF_yV_y(z)+k_xF_zV_z(z)\right]\\ p_y(z)&=-\mu_0\left(\nabla\times\boldsymbol{j}^{\mathbf{ext}}\right)_y\\ &=\mu_0\sigma_1\left[k_yF_xV_x(z)+k_yF_yV_y(z)+k_yF_zV_z(z)\right]\\ p_z(z)&=-\mu_0\left(\nabla\times\boldsymbol{j}^{\mathbf{ext}}\right)_z\\ &=\mu_0\sigma_1\begin{bmatrix}k_xF_xV_z(z)+k_yF_yV_z(z)\\ -(k_xV_x(z)+k_yV_y(z))F_z\end{bmatrix}\end{aligned} \quad (11)$$

$p_z'(z)$ denotes the derivative of $p_z(z)$ with respect to $z$ and can be described as:

$$p_z'(z)=-\mu_0\sigma_1k^2\left(V_xF_x+V_yF_y+V_zF_z\right) \quad (12)$$

From (3) and (7), the electric field $\boldsymbol{E}$ can be calculated by the magnetic flux density $\boldsymbol{B}$:

$$\boldsymbol{E}=\frac{\frac{1}{\mu_0}\nabla\times\boldsymbol{B}-\delta\boldsymbol{j}^{\mathbf{ext}}}{\sigma+i\omega\varepsilon} \quad (13)$$

Supposing that:

$$\begin{aligned}q_x(z)&=\mu_0 j_x^{\mathrm{ext}}(z)\\ q_y(z)&=\mu_0 j_y^{\mathrm{ext}}(z)\\ q_z(z)&=\mu_0 j_z^{\mathrm{ext}}(z)\end{aligned} \quad (14)$$

The general analytical solutions for the $x$, $y$ and $z$ components of the magnetic flux density $\boldsymbol{B}$ and electric field $\boldsymbol{E}$ in Layer $j$ can be written as:

$$\begin{aligned}B_x&=\sum\begin{bmatrix}a_{xj}e^{k_jz}+b_{xj}e^{-k_jz}\\ +\frac{\delta}{i\omega m_j}p_x(z)\end{bmatrix}e^{i\omega t-k_xx-k_yy}\\ B_y&=\sum\begin{bmatrix}a_{yj}e^{k_jz}+b_{yj}e^{-k_jz}\\ +\frac{\delta}{i\omega m_j}p_y(z)\end{bmatrix}e^{i\omega t-k_xx-k_yy}\\ B_z&=\sum\begin{bmatrix}a_{zj}e^{k_jz}+b_{zj}e^{-k_jz}\\ +\frac{\delta}{i\omega m_j}p_z(z)\end{bmatrix}e^{i\omega t-k_xx-k_yy}\end{aligned} \quad (15)$$

$$\begin{aligned}E_x&=\frac{1}{m_j}\sum\begin{bmatrix}-(a_{yj}k_j+a_{zj}k_y)e^{k_jz}\\ +\left(b_{yj}k_j-b_{zj}k_y\right)e^{-k_jz}\\ +\delta q_x(z)\end{bmatrix}e^{i\omega t-k_xx-k_yy}\\ E_y&=\frac{1}{m_j}\sum\begin{bmatrix}(a_{xj}k_j+a_{zj}k_x)e^{k_jz}\\ +\left(b_{zj}k_x-b_{xj}k_j\right)e^{-k_jz}\\ +\delta q_y(z)\end{bmatrix}e^{i\omega t-k_xx-k_yy}\\ E_z&=\frac{1}{m_j}\sum\begin{bmatrix}(a_{xj}k_y-a_{yj}k_x)e^{k_jz}\\ +\left(b_{xj}k_y-b_{yj}k_x\right)e^{-k_jz}\\ +\delta q_z(z)\end{bmatrix}e^{i\omega t-k_xx-k_yy}\end{aligned} \quad (16)$$

The solutions show that each component of the induced electromagnetic field is related to all three components of the velocity and geomagnetic field.

$a_{x0}$ to $b_{zN}$ are integration constants. A $N+1$ layer model containing Layer 0 has $6(N+1)$ constants. The analytical solution of those constants is very complex, but it can be solved numerically if other variables in the model are provided.

Since the induced fields tend to zero as $z$ approaches $\pm\infty$, the following can be obtained:

$$b_{x0}=b_{y0}=b_{z0}=a_{xN}=a_{yN}=a_{zN}=0 \quad (17)$$

By implementing the boundary conditions of the horizontal layers, the remaining $6N$ constants can be solved. At $N$ interfaces, the continuity of $B_x$, $B_y$ and $B_z$ can contribute $3N$ equations. $E_x$ and $E_y$ can contribute $2N$ equations. $B_z'$, the derivative of $B_z$ with respect to $z$, can contribute $N$ equations as well. Hence, $6N$ integration constants exactly satisfy $6N$ linear equations at the interfaces of $z=0,z_1,z_2,\cdots,z_j,\cdots,z_{N-1}$, in which $z_j=\sum_{i=1}^{j}h_i$.

By moving all of the first and second terms to the left-hand side of (15) and (16), we can extract both exponential and coefficient parts to formulate the coefficient matrix $\boldsymbol{A}$, which has dimensions of $6(N+1)\times 6(N+1)$. Moreover, the integration constants can be extracted to create Matrix $\boldsymbol{X}$, which has dimensions of $6(N+1)\times 1$. $\boldsymbol{X}$ contains six known integral constants in Equation (17) to facilitate the arrangement and calculation of the matrix elements. Meanwhile, we move all third terms to the right-hand side of the equations to create Matrix $\boldsymbol{b}$, which has dimensions of $6(N+1)\times 1$. At both the sea surface and seafloor, the element in $\boldsymbol{b}$ depends upon the

velocity vector of ocean waves and geomagnetic field vector. However, it is zero at the interfaces among the seabed layers. The linear equations can be written as:

$$\begin{aligned} \boldsymbol{AX} &= \boldsymbol{b} \\ \boldsymbol{X} &= \boldsymbol{A^{-1}b} \end{aligned} \tag{18}$$

The integration constants matrix is as follows:

$$\boldsymbol{X} = \begin{matrix}[a_{x0}, b_{x0}, a_{y0}, b_{y0}, a_{z0}, b_{z0}, \cdots, \\ a_{xj}, b_{xj}, a_{yj}, b_{yj}, a_{zj}, b_{zj}, \cdots, b_{xN}, b_{yN}, b_{zN}]^{\mathrm{T}}\end{matrix} \tag{19}$$

Matrix $\boldsymbol{A}$ can be denoted as Block Matrix $\boldsymbol{A} = [\boldsymbol{A_1}, \boldsymbol{A_2}, \boldsymbol{A_3}, \boldsymbol{A_4}, \boldsymbol{A_5}, \boldsymbol{A_6}, ]^{\mathrm{T}}$. Submatrix $\boldsymbol{A_i}$ corresponds to $B_x, B_y, B_z, B_z', E_x$, and $E_y$, respectively, and its matrix dimension is $(N+1) \times 6(N+1)$. Meanwhile, Matrix $\boldsymbol{b}$ can also be denoted as Block Matrix $\mathrm{b} = [\boldsymbol{b_1}, \boldsymbol{b_2}, \boldsymbol{b_3}, \boldsymbol{b_4}, \boldsymbol{b_5}, \boldsymbol{b_6}]^{\mathrm{T}}$, and its matrix dimension of $\boldsymbol{b_i}$ is $(N+1) \times 1$.

Submatrix $\boldsymbol{A_i}$ is a banded matrix. The expression of the nonzero elements of Row $1 \leq j \leq \mathrm{N}+1$ in Submatrix $\boldsymbol{A_i}$ is as follows:

$$\begin{aligned}
&\boldsymbol{A_1}(\mathrm{j}, 6\mathrm{j}-5) = \boldsymbol{A_2}(\mathrm{j}, 6\mathrm{j}-3) = \boldsymbol{A_3}(\mathrm{j}, 6\mathrm{j}-1) = e^{k_{j-1}z_{j-1}} \\
&\boldsymbol{A_1}(\mathrm{j}, 6\mathrm{j}-4) = \boldsymbol{A_2}(\mathrm{j}, 6\mathrm{j}-2) = \boldsymbol{A_3}(\mathrm{j}, 6\mathrm{j}) = e^{-k_{j-1}z_{j-1}} \\
&\boldsymbol{A_1}(\mathrm{j}, 6\mathrm{j}+1) = \boldsymbol{A_2}(\mathrm{j}, 6\mathrm{j}+3) = \boldsymbol{A_3}(\mathrm{j}, 6\mathrm{j}+5) = -e^{k_j z_{j-1}} \\
&\boldsymbol{A_1}(\mathrm{j}, 6\mathrm{j}+2) = \boldsymbol{A_2}(\mathrm{j}, 6\mathrm{j}+4) = \boldsymbol{A_3}(\mathrm{j}, 6\mathrm{j}+6) = -e^{-k_j z_{j-1}} \\
&\boldsymbol{A_4}(\mathrm{j}, 6\mathrm{j}-1) = k_{j-1}e^{k_{j-1}z_{j-1}} \\
&\quad \boldsymbol{A_4}(\mathrm{j}, 6\mathrm{j}) = -k_{j-1}e^{-k_{j-1}z_{j-1}} \\
&\boldsymbol{A_4}(\mathrm{j}, 6\mathrm{j}+5) = -k_j e^{k_j z_{j-1}} \\
&\boldsymbol{A_4}(\mathrm{j}, 6\mathrm{j}+6) = k_j e^{-k_j z_{j-1}} \\
&\boldsymbol{A_5}(\mathrm{j}, 6\mathrm{j}-5) = \boldsymbol{A_6}(\mathrm{j}, 6\mathrm{j}-3) = (k_{j-1}/m_{j-1})e^{k_{j-1}z_{j-1}} \\
&\boldsymbol{A_5}(\mathrm{j}, 6\mathrm{j}-4) = \boldsymbol{A_6}(\mathrm{j}, 6\mathrm{j}-2) = (-k_{j-1}/m_{j-1})e^{-k_{j-1}z_{j-1}} \\
&\boldsymbol{A_5}(\mathrm{j}, 6\mathrm{j}+1) = \boldsymbol{A_6}(\mathrm{j}, 6\mathrm{j}+3) = (-k_j/m_j)e^{k_j z_{j-1}} \\
&\boldsymbol{A_5}(\mathrm{j}, 6\mathrm{j}+2) = \boldsymbol{A_6}(\mathrm{j}, 6\mathrm{j}+4) = (k_j/m_j)e^{-k_j z_{j-1}} \\
&\boldsymbol{A_5}(\mathrm{j}, 6\mathrm{j}-1) = (k_x/m_{j-1})e^{k_{j-1}z_{j-1}} \\
&\quad \boldsymbol{A_5}(\mathrm{j}, 6\mathrm{j}) = (k_x/m_{j-1})e^{-k_{j-1}z_{j-1}} \\
&\boldsymbol{A_5}(\mathrm{j}, 6\mathrm{j}+5) = (-k_x/m_j)e^{k_j z_{j-1}} \\
&\boldsymbol{A_5}(\mathrm{j}, 6\mathrm{j}+6) = (-k_x/m_j)e^{-k_j z_{j-1}} \\
&\boldsymbol{A_6}(\mathrm{j}, 6\mathrm{j}-1) = (k_y/m_{j-1})e^{k_{j-1}z_{j-1}} \\
&\quad \boldsymbol{A_6}(\mathrm{j}, 6\mathrm{j}) = (k_y/m_{j-1})e^{-k_{j-1}z_{j-1}} \\
&\boldsymbol{A_6}(\mathrm{j}, 6\mathrm{j}+5) = (-k_y/m_j)e^{k_j z_{j-1}} \\
&\boldsymbol{A_6}(\mathrm{j}, 6\mathrm{j}+6) = (-k_y/m_j)e^{-k_j z_{j-1}}
\end{aligned}$$

The element in Matrix $\boldsymbol{b_i}$ can be written as:

$$\boldsymbol{b_1} = \frac{1}{i\omega m_1}\left[\underbrace{p_x(0), -p_x(z_1), 0, \cdots, 0, \quad \cdots, 0}_{N+1}\right]^{\mathrm{T}}$$

$$\boldsymbol{b_2} = \frac{1}{i\omega m_1}\left[\underbrace{p_y(0), -p_y(z_1), 0, \cdots, 0, \quad \cdots, 0}_{N+1}\right]^{\mathrm{T}}$$

$$\boldsymbol{b_3} = \frac{1}{i\omega m_1}\left[\underbrace{p_z(0), -p_z(z_1), 0, \cdots, 0, \quad \cdots, 0}_{N+1}\right]^{\mathrm{T}}$$

$$\boldsymbol{b_4} = \frac{1}{i\omega m_1}\left[\underbrace{p_z'(0), -p_z'(z_1), 0, \cdots, 0, \quad \cdots, 0}_{N+1}\right]^{\mathrm{T}}$$

$$\boldsymbol{b_5} = \frac{1}{m_1}\left[\underbrace{q_y(0), -q_y(z_1), 0, \cdots, 0, \quad \cdots, 0}_{N+1}\right]^{\mathrm{T}}$$

$$\boldsymbol{b_6} = \frac{1}{m_1}\left[\underbrace{-q_x(0), q_x(z_1), 0, \cdots, 0, \quad \cdots, 0}_{N+1}\right]^{\mathrm{T}} \tag{20}$$

Each expression is simple and regular. Once other model parameters are provided, all the integral constants can be solved. Using the integral constants, we can easily evaluate the electromagnetic field at an arbitrary position from the information of the 3-D ocean waves and the electrical conductivity structure by a simpler and more direct method rather than a cumbersome integral.

### B. VELOCITY VECTOR OF OCEAN WAVES

We employ a linear superimposed 3-D ocean wave model [17] to simulate a real sea environment. The sea wave elevation $\zeta(x, y, t)$ can be represented as the sum of the cosine wave components:

$$\zeta(x, y, t) = \sum_{m=1}^{M}\sum_{n=1}^{N} a(\omega_m, \theta_n)\cos(\omega_m t - k_m \cos\theta_n x - k_m \sin\theta_n y + \varepsilon_{m,n}) \tag{21}$$

where $a(\omega_m, \theta_n)$, $\omega_m$, $k_m$, $\theta_n$, and $\varepsilon_{m,n}$ denote the amplitude, angular frequency, wavenumber, propagation direction, and initial phases in various components, respectively. $\varepsilon_{m,n}$ is randomly distributed in $(0, 2\pi)$.

Within the realm of linear wave theory, the analytical solution of the velocity potential related to 3-D ocean waves in a sea of finite depth can be derived [18]:

$$\varphi(x, y, z, t) = -A(\omega, \theta)\,\mathrm{Cosh}[k(h_1 - z)]\, e^{i\omega t - k_x x - k_y y} \tag{22}$$

Seawater is assumed to be incompressible and irrotational, and thus, the magnetic flux density satisfies $\nabla \cdot \boldsymbol{V} = 0$ and $\nabla \times \boldsymbol{V} = 0$. Using $V = -\nabla\varphi$, three components of velocity can be obtained:

$$\begin{aligned}
V_x(x, y, z, t) &= A(\omega, \theta)\, k_x \mathrm{Cosh}[k(h_1 - z)]\, e^{i\omega t - k_x x - k_y y} \\
V_y(x, y, z, t) &= A(\omega, \theta)\, k_y \mathrm{Cosh}[k(h_1 - z)]\, e^{i\omega t - k_x x - k_y y} \\
V_z(x, y, z, t) &= A(\omega, \theta)\, k \mathrm{Sinh}[k(h_1 - z)]\, e^{i\omega t - k_x x - k_y y}
\end{aligned} \tag{23}$$

in which $A(\omega, \theta) = -a(\omega, \theta)g/(\omega \mathrm{Cosh}(kh_1))$

The angular frequency $\omega$ and wavenumber $k$ satisfy the dispersion relation:

$$\omega^2 = gk\,\mathrm{Tanh}(kh_1) \tag{24}$$

$a(\omega, \theta)$, the amplitude of the wave component, can be determined by using the ocean wave directional spectrum, which denotes the relationship between energy and both the frequency and direction of ocean waves:

$$a(\omega, \theta) = \sqrt{2S(\omega)} G(\omega, \theta - \alpha) \Delta\theta \tag{25}$$

where $\Delta\theta = \pi/N$.

$S(\omega)$ denotes the relationship between the energy and frequency of ocean waves. Moreover, we use the P-M spectrum [19]:

$$S(\omega) = \frac{\lambda g^2}{\omega^5} \exp\left[-\beta\left(\frac{g}{\omega U_{19.5}}\right)^4\right] \tag{26}$$

where $\lambda = 8.1\times10^{-3}$, $\beta = 0.74$ and $U_{19.5}$ denotes the wind speed at an altitude of 19.5 m above the sea surface.

We use the SWOP direction function in $G(\omega, \theta)$ [20] to denote the energy distribution in different wave directions:

$$G(\omega, \theta) = \frac{1}{\pi}(1 + a\cos 2\theta + b\cos 4\theta) \quad |\theta| \le \frac{\pi}{2} \tag{27}$$

where $a = 0.5 + 0.82\exp\left[-\omega^4/2\omega_p^4\right]$, $b = 0.32\exp\left[-\omega^4/2\omega_p^4\right]$, and $\omega_p$ is the peak frequency of $S(\omega)$.

## III. SIMULATION EXAMPLES AND DISCUSSION

### A. SPATIAL DISTRIBUTION

From Fig. 2, we consider a 1D three-layer electrical conductivity model consisting of a 3.3 S/m seawater with a varying depth $h_1$, a 1000 m thick sediment layer with varying electrical conductivity $\sigma_2$ below the seafloor, and a 0.1 S/m bottom layer extending indefinitely. A $10^{-12}$ S/m air layer extends indefinitely as well.

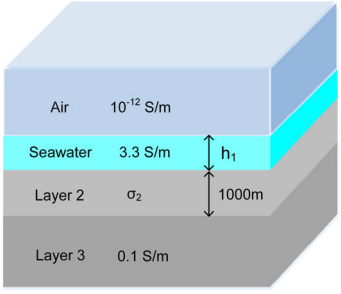


**FIGURE 2.** A 1D electrical conductivity model.

Here, we suppose that the three components of the geomagnetic field have the same value to avoid the influence of the ambient field; thus, the inclination $I$ satisfies $sinI = \sqrt{3}/3$, and the deviation of geomagnetic north is $\phi = 45°$. Moreover, we assume that the intensity of the geomagnetic field is $F = 5\times10^4$nT. The wind direction is $\alpha = 60°$. Additionally, we deduce that $x = y = t = 0$ without loss of generality.

Fig. 3 shows the electromagnetic response in seawater for five wave periods ($T$ = 5 s, 7 s, 10 s, 13 s, 15s). The water depth is $h_1 = 500$m, and the electrical conductivity of the sediment layer is $\sigma_2 = 1$S/m. A typical wind speed at 10 m above the sea surface is set to $U_{10} = 12$m/s, which represents a strong breeze, corresponding to Beaufort scale 6 [21]. Ocean waves generate a magnetic flux density less than a couple of nT, and the electric field can reach several tens of microvolts per meter ($\mu$V/m) at the sea surface. Generally, the motional fields can propagate no more than 300 m. $B_x$ and $B_y$ decrease first with depth but increase after reaching their minimum and finally decay to zero after reaching their maximum. $B_z$ first increases slowly but sharply decays to zero after reaching its maximum. Meanwhile, $E_x$, $E_y$, and $E_z$ monotonically decay to zero with depth. The longer the period is, the deeper the location of both maxima and minima within the sea, and the slower the field decay rate. A more detailed discussion related to maxima and minima has been presented in [15].

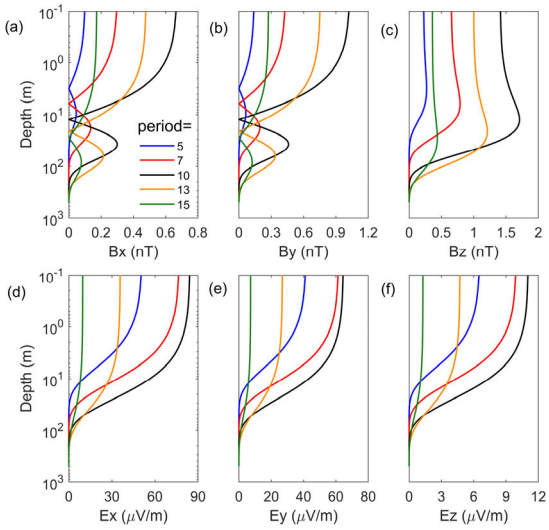


**FIGURE 3.** Electromagnetic response in seawater for various wave periods (5 *s*, 7 *s*, 10 *s*, 13 *s*, 15*s*). The sea water depth is $h_1 = 500m$, and the electrical conductivity of the sediment layer is $\sigma_2 = 1S/m$. The wind speed at 10 m above the sea surface is $U_{10} = 12m/s$.

Fig. 3 also shows that $B_z$ is stronger than both $B_x$ and $B_y$. However, $E_z$ is smaller than both $E_x$ and $E_y$ if the values of the three components of the geomagnetic field are the same. To see the influence of the geomagnetic field on the electromagnetic response, we calculate the amplitude ratio of the vertical component to the horizontal component with varying geomagnetic inclination. We suppose that the wind direction is angled at $\alpha = 30°, 60°, 45°$ as shown in Figs. 4 and 5. The wave period is $T = 10$s.

As shown in Figs. 4 and 5, both $B_z/B_x$ and $B_z/B_y$ are always greater than 1, but $E_z/E_x$ and $E_z/E_y$ are lower than 1 with inclination from $0^\circ$ to $90^\circ$. The vertical magnetic flux density is invariably larger than the horizontal magnetic flux density regardless of the value of inclination. This is because the vertical geomagnetic field has one more contribution in $B_z$ than in both $B_x$ and $B_y$, as seen in (11) and (15). In sharp

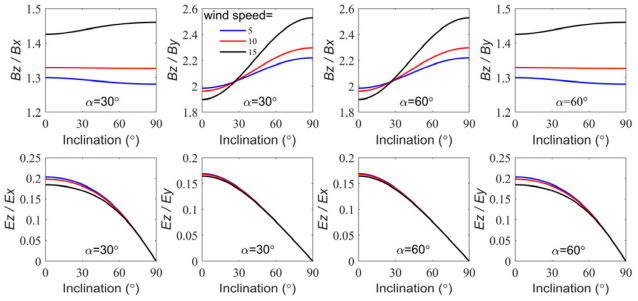


**FIGURE 4.** The amplitude ratio of the vertical component to the horizontal component at the sea surface with inclination varying from 0° to 90°. Wind direction at $\alpha = 30°$ (left panels) and $\alpha = 60°$ (right panels).

contrast to the magnetic flux density, the vertical electric field is always much smaller than the horizontal electric field, which is a consequence of cancelling in two horizontal velocities, the values of which are very close, as seen in (5), (14), and (16).

Figs. 4 and 5 also show that the larger the inclination is, the smaller the ratio of $E_z/E_x$ and $E_z/E_y$ is. In particular, the ratio tends to zero when the wind direction is oriented at $\alpha = 45°$ because $E_z$ tends to zero if two horizontal velocities almost completely cancel, as shown in Equation (5). However, this effect is complicated in a magnetic flux density. It is obvious only if the angle between the horizontal magnetic flux density and wind direction is relatively large; the larger the inclination is, the smaller the ratio is. Otherwise, the inclination barely affects the ratio. Additionally, the wind speed barely affects the ratio in the electric field but clearly affects the ratio in the magnetic flux density.

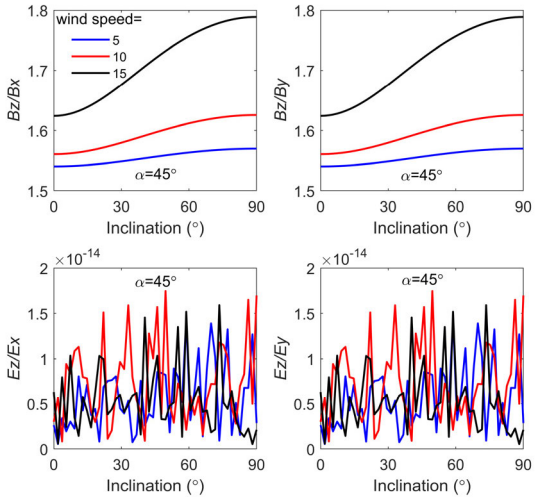


**FIGURE 5.** Same as Figure 4 but for wind direction at $\alpha = 45°$.

To see how both the wind field and geomagnetic field affect the relationship between the two horizontal components of the induced field, we calculate $B_x/B_y$ and $E_x/E_y$ at the sea surface, with the deviation of geomagnetic north at $\phi = 45°$ and simultaneous wind direction $\alpha$ varying from 0° to 90° for this case and $\alpha = 45°$ and simultaneous $\phi$ varying from 0° to 90° for another case. As shown in Fig. 6, the horizontal component that is closer to the wind direction or geomagnetic north is greater than its orthogonal horizontal component in the magnetic flux density. It contrasts to two horizontal electrical fields as well because the horizontal electrical field is contributed from the horizontal magnetic flux density that is orthogonal to it. $B_x/B_y$ and $E_x/E_y$ are 1 if simultaneously $\alpha = 45°$ and $\phi = 45°$. Moreover, the effect of the wind direction on the ratio in the magnetic flux density is more obvious than the effect of geomagnetic deviation.

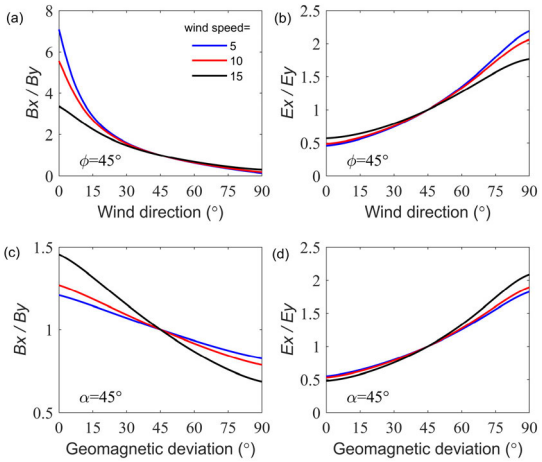


**FIGURE 6.** Amplitude ratio of $B_x/B_y$ and $E_x/E_y$ at the sea surface, with $\phi = 45°$ and $\alpha$ varying from 0° to 90° (top panels) and with $\alpha = 45°$ and $\phi$ varying from 0° to 90° (bottom panels).

Strictly speaking, motion induction, driven by the velocity of seawater and the geomagnetic field, is independent of the recording geometry, and only the amplitude of the observed electromagnetic field undoubtedly is closely dependent upon that.

### B. FREQUENCY SPECTRUM AND TIME SERIES

A particularly important phenomenon that appears in Fig. 3 is that the amplitude of motional fields caused by short ocean waves is not monotonic with the period. For example, the amplitudes of motional fields generated by ocean waves with periods of 5 s and 15 s are smaller than those generated by ocean waves with a period of 10 s. To theoretically simulate the frequency spectrum of induced fields is significant. Here, we use 1000 discrete frequency components, and the corresponding periods range from 1 s to 1000 s. By using the directional spectrum and dispersion relation, we calculate the wave amplitude $a$ and wavenumber $k$. Moreover, we suppose that $I = 30°$, $\phi = 45°$, $\alpha = 60°$, the water depth is $h_1 = 500$m, and the conductivity of the sediment layer is $\sigma_2 = 1$S/m.

Fig. 7 shows the frequency spectrum for three wind speeds ($U_{10} = 12$m/s, 15m/s, 18m/s) at $z = 0$ m and $z = 50$ m. Notably, the motional fields have a narrow band spectrum. The magnetic and electrical fields mainly lie at 0.04-0.3 Hz

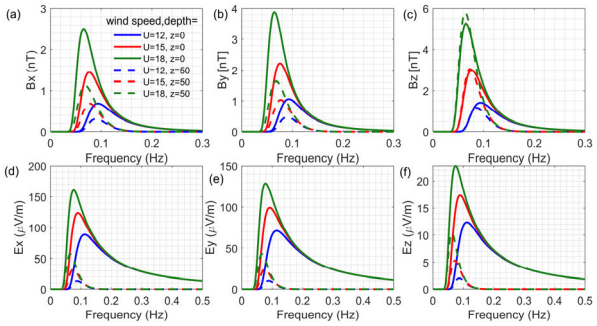


**FIGURE 7.** The frequency spectrum of electromagnetic fields induced by 3-D ocean waves for various wind speeds at $z = 0$ m and $z = 50$ m. A series of 1,000 periods ranging from 1 s to 1,000 s. The water depth is $h_1 = 500m$, and the electrical conductivity of the sediment layer is $\sigma_2 = 1S/m$. $I = 30^\circ$, $\phi = 45^\circ$, $\alpha = 60^\circ$.

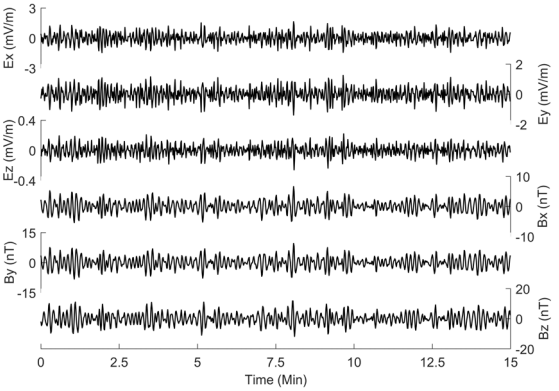


**FIGURE 8.** The 15-minute time series of the electromagnetic fields induced by 3-D ocean waves at $z = 0$ m. The sampling frequency is $Fs = 1$ Hz, and the number of sampling points is 900. The water depth is $h_1 = 500m$ and the electrical conductivity of the sediment layer is $\sigma_2 = 1S/m$. The wind speed is set to be $U_{10} = 10m/s$.

and 0.04-0.5 Hz at the sea surface, respectively, namely, the periods are approximately distributed from 2-30 s. Both are in a narrower band of 0.04-0.15 Hz at $z = 50$ m, namely, the periods are approximately 6-30 s. The spectra have a peak frequency, where the amplitude of the fields is largest, and do not vary with depth. On the other hand, the deeper the position is, the narrower the band, which moves toward a lower frequency, and the lower magnitude the fields have. The attenuation of the high-frequency component is more significant in the electrical field than in the magnetic flux density with increasing depth.

Fig. 7 also shows that wind above the sea surface obviously affects the spectrum. The larger the wind speed is, the greater magnitude the fields have, the lower the peak frequency is, and the wider the frequency band becomes. The wider band appears in the lower frequency component.

Usually, the first-hand field data we observe are in the time domain. Simulated data in the time domain are also needed in some studies, such as signal processing. Here, we theoretically simulate the time series of motional fields caused by short ocean waves as well. To reflect the initial phase's randomness of the field without changing its amplitude, we multiply each frequency component of the spectrum by an exponential term $e^{i\varepsilon}(|e^{i\varepsilon}| \equiv 1)$ in which $\varepsilon$ is uniformly distributed in the interval $(0, 2\pi)$. Then, we use the complex conjugate symmetrical spectrum. We perform a fast Fourier transform (FFT) to simulate the time series of fields.

We simulate that the time series is 15 minutes long and suppose that the sampling frequency is Fs = 1 Hz; thus, the sampling points are 900. Of course, we can simulate data of arbitrary sampling frequency and arbitrary sampling length. Here, the wind speed is set to $U_{10} = 10$m/s. The water depth is $h_1 = 500$m, and the electrical conductivity of the sediment layer is $\sigma_2 = 1$S/m.

Figs. 8 and 9 show clear periodicity at the sea surface and within the sea for noise-free data. Moreover, the motional fields vary simultaneously in time as a quasi-sinusoidal period of approximately a few seconds. Random noise can be added to simulate a more realistic marine environment if needed. Six components are mainly distributed at ±2 mV/m, ±2 mV/m, ±0.4 mV/m, ±7 nT, ±8 nT, and ±12 nT at the sea surface. The amplitude is smaller at z = 50 m than at the sea surface, largely ranging in ±0.1 mV/m, ±0.1 mV/m, ±0.02 mV/m, ±2 nT, ±3 nT, and ±5 nT, respectively. Even if the magnitude of extrema in the time domain is much greater than that in the frequency domain, smaller values account for the majority of the sequence. Fluctuating more frequently at the sea surface than within the sea, both electrical and magnetic flux density have higher frequency components at the sea surface. Hence, the data in the time domain can reflect field attenuation in seawater as well.

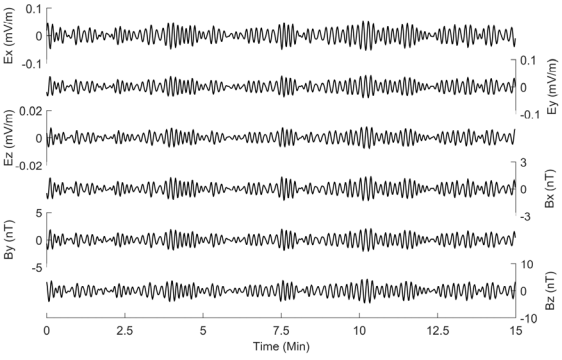


**FIGURE 9.** Same as Figure 8 but at $z = 50m$.

### C. POSSIBILITY OF DETECTING SEAFLOOR CONDUCTIVITY STRUCTURES BY USING THE ELECTROMAGNETIC RESPONSE OF OCEAN WAVES

Before analyzing the possibility, we first discuss the influence of ocean thickness on motional fields to determine the conditions under which the finite sea can be assumed to be infinite when involving the motion induction of ocean waves.

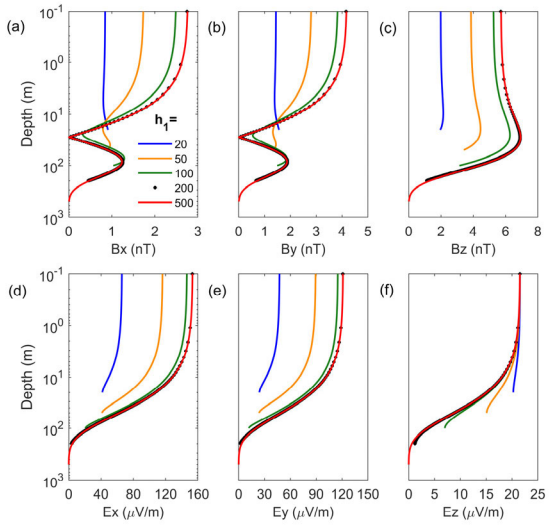


**FIGURE 10.** Electromagnetic response in seawater for various water depths. The electrical conductivity of the sediment layer is $\sigma_2 = 1S/m$. The wave period is $T = 15s$. The wind speed is $U_{10} = 18m/s$.

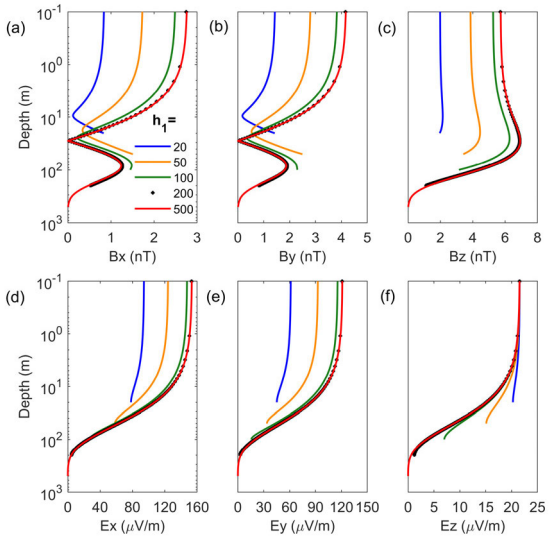


**FIGURE 11.** As in Figure 10, but for the electrical conductivity of the sediment layer at $\sigma_2 = 0.001\ S/m$.

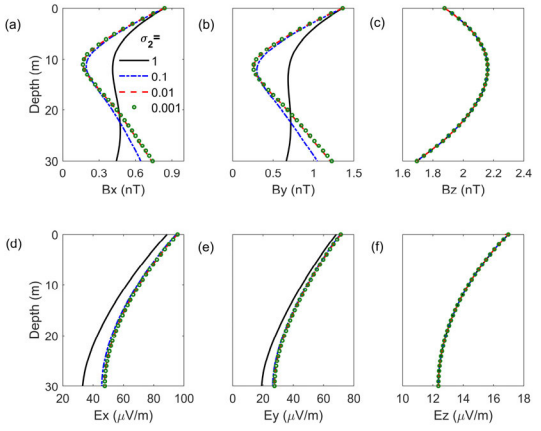


**FIGURE 12.** Electromagnetic response in seawater for various values of electrical conductivity of the sediment layer. The sea water depth is $h_1 = 30m$, and the wave period is T = 12 s. The wind speed at 10 m above the sea surface is set to $U_{10} = 15m/s$.

Fig. 10 shows the response in seawater for five water depths ($h_1$ = 20 m, 50 m, 100 m, 200 mand500 m). Moreover, we determine that $\sigma_2 = 1$S/m and $T = 15$s. A higher wind speed is set to $U_{10} = 18$m/s (gale, corresponding to Beaufort scale 8). Fig.11 as Fig.10 but for $\sigma_2 = 0.001$ S/m. The thickness of seawater affects the fields' distribution and magnitude until it is larger than 200 m, whether it is a high resistivity or high conductivity seabed beneath the sea. Under a gale sea state, at the sea surface, the difference between 20 m- and 200 m-thick seas can reach a couple of nT in the magnetic flux density and dozens of $\mu$V/m in the electrical field. One exception is that the induced vertical electrical field is barely affected by the thickness of seawater when far from the seabed. Hence, using a model of infinite sea depth to simulate induced fields generated by short ocean waves in shallow water (less than 200 m thick) is likely to produce inaccuracies that cannot be overlooked. In addition, it can be inferred that topographic relief may influence the electromagnetic response caused by short ocean waves in shallow water, such as coastal regions.

Then, we calculate the motional fields in seawater for four values of electrical conductivity of the sediment layer ($\sigma_2$ = 1S/m, 0.1 S/m, 0.01 S/m, 0.001 S/m), and the sea depth is set to $h_1 = 30$mand200 m. Moreover, we determine that $T$ = 12s and $U_{10} = 15$m/s (near gale, corresponding to Beaufort scale 7). As shown in Fig. 12, the induced fields have not decayed significantly before reaching the seafloor in the case of a 30-m sea depth. The conductivity of the seafloor layer affects the horizontal magnetic flux density and electrical field except at the sea surface. The smaller the conductivity is, the greater the horizontal fields are at the seafloor. However, the effect on the magnetic flux density decreases dramatically with continually decreasing conductivity and disappears if it is lower than 0.01S/m. The critical value of the influence on the electric field is 0.1 S/m. However, the seafloor conductivity does not affect the vertical components of motional fields at all.

As shown in Fig. 13, the magnitude has nearly decayed to zero before reaching the seafloor in the case of 200 m sea depth. At this time, the seafloor conductivity has no effect on the fields caused by short ocean waves at all. Hence, as expected, it may not be suitable to detect seafloor conductivity structures in the deep sea by using motional fields due to short ocean waves. Only if motional fields have not decayed significantly before reaching the seafloor in very shallow sea regions and the effect of seafloor conductivity is visible can we continuously discuss this possibility.

The spectrum at the seafloor corresponding to Fig. 12 is shown in Fig. 14. Since vertical motional fields are not influenced by seafloor conductivity, they are not discussed here.

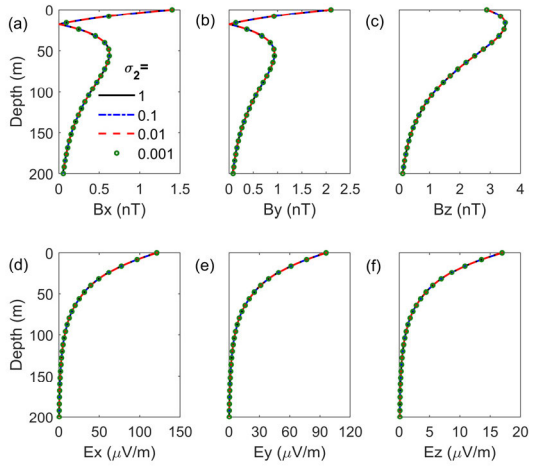


**FIGURE 13.** As in Figure 12 but for sea water depth of $h_1 = 200m$.

The effect of seabed conductivity on the field's spectrum is present in the amplitude and shape rather than the bandwidth. The spectral amplitude corresponding to the high resistivity seabed is clearly larger in both electric and magnetic flux density. As shown in the magnetic flux density, the spectral shape corresponding to the 1 S/m seabed shows an obvious asymmetry, and the peak frequency inclines to the low frequency. After passing a sharp peak, the amplitude decreases very slowly with increasing frequency compared with that corresponding to the lower conductivity seabed, which has a sharp slope at high frequencies. This can possibly be applied to identify high-conductivity seabed structures.

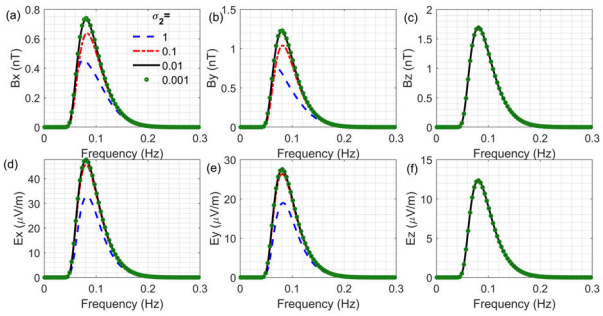


**FIGURE 14.** Frequency spectrum at the seafloor for various values of electrical conductivity of the sediment layer. The sea water depth is $h_1 = 30m$, and the wave period is T = 12 s. The wind speed at 10 m above the sea surface is set to $U_{10} = 15m/s$.

## IV. CONCLUSION

In this paper, the simulation results can be summarized as follows:

(1) For the magnetic flux density induced by three-dimensional ocean waves, the vertical component is invariably larger than the two horizontal components regardless of the value of inclination, and only if the angle between the horizontal component and wind direction is relatively large does the ratio of the vertical component to the horizontal component decrease with increasing inclination. Otherwise, the inclination barely affects the ratio. Conversely, for the electric field, the vertical component is always much smaller than the two horizontal components. Moreover, the larger the inclination is, the smaller the ratio. Additionally, the wind speed barely affects the ratio in the electric field but clearly affects the ratio in the magnetic flux density.

(2) The induced horizontal magnetic flux density closer to the wind direction or geomagnetic north has a larger value than its orthogonal horizontal component. It contrasts to two horizontal electrical fields as well. The effect of the wind direction on the ratio of both horizontal magnetic flux density is more obvious than the effect of geomagnetic deviation.

(3) The electromagnetic fields due to three-dimensional ocean waves have a narrow band spectrum. The spectrum has a peak frequency, where the amplitude of the fields is largest, and does not vary with depth. The deeper the position is, the narrower the band, which moves toward a lower frequency, and the lower magnitude the fields have, which can be seen in the results of the time series as well. The attenuation of the high-frequency component is more significant in the electrical field than in the magnetic flux density with increasing depth. The wind above the sea surface obviously affects the spectrum. The larger the wind speed is, the greater magnitude the fields have, the lower the peak frequency is, and the wider the frequency band becomes. The wider band appears in the lower frequency component.

(4) Regarding high resistivity or high conductivity seabeds, the thickness of seawater affects the induced fields' distribution and magnitude until it is larger than 200 m. One exception is that the induced vertical electrical field is barely affected by the thickness of seawater when far from the seabed. Using a model of infinite sea depth to simulate induced fields generated by ocean waves in shallow water (less than 200 m) is likely to produce inaccuracies that cannot be overlooked, and topography may influence on the electromagnetic response caused by short ocean waves in shallow water, such as coastal regions.

(5) Only if motional fields have not decayed significantly before reaching the sea floor in a region of very shallow sea and the effect of seafloor conductivity is visible can the possibility of detecting seafloor conductivity structures be discussed by using the electromagnetic response related to short ocean waves. Moreover, the shape of the spectrum of the induced horizontal components at the seafloor, especially the magnetic flux density, can be applied to identify high-conductivity seabed structures.

## REFERENCES

[1] Y. Wu, M. Luo, Y. Li, J. Ge, and L. Pan, "A method for reducing ocean wave-induced magnetic noises in shallow-water MT data using a complex adaptive filter," *J. Ocean Univ. China*, vol. 22, no. 1, pp. 99–106, Jan. 2023.

[2] C. Feng, Y. Li, Y. Wu, and S. Duan, "A noise suppression method of marine magnetotelluric data using K-SVD dictionary learning," *Chin. J. Geophys.*, vol. 65, no. 5, pp. 1853–1865, May 2022.

[3] S. Duan, Y. Li, J. Pei, T. Zhao, Z. Wu, B. Han, X. Yu, L. Liu, J. Chen, and Z. Xu, "Carbonate imaging with magnetotellurics in a shallow-water environment, South Yellow Sea, China," *J. Appl. Geophys.*, vol. 178, Jul. 2020, Art. no. 104076.
[4] K. Chen, Q. Zhao, M. Deng, X. Luo, and J. Jing, "Seawater motion-induced electromagnetic noise reduction in marine magnetotelluric data using current meters," *Earth, Planets Space*, vol. 72, no. 1, p. 4, Jan. 2020.
[5] P. Cui, J. Lv, J. Shao, and S. Pang, "Comparative analysis of contribution degree of environmental parameters in wave induced magnetic field," in *Proc. IEEE 4th ICCSSE*, Wuhan, China, Aug. 2018, pp. 236–241.
[6] H. Shimizu and H. Utada, "Motional magnetotellurics by long oceanic waves," *Geophys. J. Int.*, vol. 201, no. 1, pp. 390–405, Feb. 2015.
[7] K. M. Bhatt, "Motion induced noise in marine electromagnetic data," Ph.D. dissertation, Faculty Elect. Eng., Inf. Technol., Phys., Tech. Univ., Braunschweig, Germany, 2011.
[8] D. Tilley, M. Dhanak, E. An, and K. Von Ellenrieder, "Characterizing magnetic sensors and magnetic noise of AUVs," in *Proc. Oceans*, Hampton Roads, VA, USA, Oct. 2012, pp. 1–5.
[9] Y. Shen, J. Wang, and J. Gao, "Noise suppression for vector magnetic anomaly detection by noise spatial characteristics investigation," *IEEE Geosci. Remote Sens. Lett.*, vol. 19, pp. 1–4, 2022.
[10] X. Xiong, R. J. Yang, and K. L. Miao, "Simulation of ocean wave-generated magnetic field disturbance observed above sea-surface based on directional spectrum," *Adv. Mater. Res.*, vols. 791–793, pp. 1139–1144, Sep. 2013.
[11] J. B. Nelson, *Detecting Wave-Induced Magnetic Signals With an Airborne Magnetometer*, document DRDC Atlantic Technical Memorandum 2002-209, 2002.
[12] J. B. Nelson, *Aeromagnetic Noise During Low-Altitude Flights Over the Scotian Shelf*, document DRDC Atlantic technical Memorandum 2002-089, 2002.
[13] F. E. M. Lilley, A. P. Hitchman, P. R. Milligan, and T. Pedersen, "Sea-surface observations of the magnetic signals of ocean swells," *Geophys. J. Int.*, vol. 159, no. 2, pp. 565–572, Nov. 2004.
[14] J. A. Kluge, A. V. Soloviev, C. W. Dean, G. K. Morrison, and B. K. Haus, "Analysis of the magnetic signature of surface waves measured in a laboratory experiment," *J. Atmos. Ocean. Technol.*, vol. 39, no. 5, pp. 641–648, May 2022.
[15] J. T. Weaver, "Magnetic variations associated with ocean waves and swell," *J. Geophys. Res.*, vol. 70, no. 8, pp. 1921–1929, Apr. 1965.
[16] T. Minami, "Motional induction by tsunamis and ocean tides: 10 years of progress," *Surveys Geophys.*, vol. 38, no. 5, pp. 1097–1132, Jun. 2017.
[17] M. S. Longuet-Higgins, "On the statistical distribution of the heights of sea waves," *J. Mar. Res.*, vol. 11, no. 3, pp. 245–266, Jan. 1952.
[18] A. Ye and F. Li, *Physical Oceanography*. Qingdao, China: Qingdao Ocean University, 1992.
[19] W. J. Pierson and L. Moskowitz, "A proposed spectral form for fully developed wind seas based on the similarity theory of S. A. Kitaigorodskii," *J. Geophys. Res.*, vol. 69, no. 24, pp. 5181–5190, Dec. 1964.
[20] J. Chase, "The directional spectrum of a wind generated sea as determined from data obtained by the Stereo Wave Observation Project," College Eng., New York Univ., New York, NY, USA, Tech. Rep. 6, 1960.
[21] G. Verploegh and N. M. I. Koninklijk, "The equivalent velocities for the Beaufort estimates of the wind force at sea," Staatsdrukkerij-en Uitgeverijbedrijf, The Hague, The Netherlands, Tech. Rep. 66, pp. 1–38, 1956.

**RONGHUA TAO** was born in Yancheng, China, in 1971. He received the B.S. degree in photogrammetry and remote sensing, the M.Sc. degree in underwater acoustic engineering, and the Ph.D. degree in naval architecture and marine engineering from Navy Submarine Academy, Qingdao, China, in 1998, 2001, and 2015, respectively.

He is currently a Professor with Navy Submarine Academy. His current research interests include remote sensing image processing and signal detection.

**BAOQIANG ZHANG** was born in Pingliang, China, in 1992. He received the B.S. degree in exploration technology and engineering and the M.Sc. degree in geological engineering from the Ocean University of China, Qingdao, China, in 2015 and 2018, respectively. Since 2023, he has been pursuing the Ph.D. degree in electronic information with Qingdao Innovation and Development Base, Harbin Engineering University, Qingdao.

He was a Research and Development Engineer with CSSC Ocean Exploration Technology Research Institute Company Ltd. He is currently an Engineer with Qingdao Institute of Collaborative Innovation, Qingdao. His current research interests include modeling, simulation and data processing of magnetic anomalies, extremely low-frequency (ELF), wake, and motion-induced electromagnetic fields.

**CHUN ZHOU** was born in Zhangye, China, in 1993. He received the B.S. degree in exploration technology and engineering and the M.Sc. degree in marine geophysics from the Ocean University of China, Qingdao, China, in 2016 and 2019, respectively.

He was a Research and Development Engineer with CSSC Ocean Exploration Technology Research Institute Company Ltd. He is currently an Engineer with Qingdao Institute of Collaborative Innovation, Qingdao. His current research interest includes magnetic signal processing.

**HE QIAO** was born in Yantai, China, in 1997. She received the B.S. degree in exploration technology and engineering and the M.Sc. degree in earth exploration and information technology from the Ocean University of China, Qingdao, China, in 2019 and 2022, respectively.

Her current research interests include numerical simulation on extremely low-frequency (ELF) and seawater induced electromagnetic fields.